

# **Supplementary Information for: A model of elastic softening and second order phase transitions in anisotropic phases, with application to stishovite and post-stishovite**

R. Myhill<sup>1\*</sup>

<sup>1</sup>School of Earth Sciences, University of Bristol. Wills Memorial Building, Queen's Road, Bristol BS8 1RJ

## **SUMMARY**

This paper introduces a comprehensive framework for modeling both instantaneous and time-dependent elastic softening in anisotropic materials. Like previous approaches, the framework employs Landau Theory, minimizing the Helmholtz energy by varying isochemical parameters ( $q$ ) that capture structural changes, atomic ordering, and/or electronic spin states. However, this model extends beyond earlier work by incorporating excess energy and anisotropic properties into an anisotropic solution model. This allows for fully self-consistent predictions of volume, unit cell parameters, the elastic tensor, and other thermodynamic properties as a function of pressure and temperature, while also accommodating large symmetry-breaking strains. The stishovite-to-post-stishovite transition is used as a case study to validate the formulation. It is demonstrated that, near this transition, both stishovite and post-stishovite exhibit auxetic behavior in several directions, with post-stishovite also displaying negative linear compressibility along the long axis of its unit cell.

**Key words:** Equations of state – Elasticity and anelasticity – Seismic anisotropy – Elastic softening

\* bob.myhill@bristol.ac.uk

**1 UNCERTAINTIES ON MODEL PARAMETERS**

In the main text, I decided not to include estimates of the uncertainties on the parameters. This was primarily because in large multiparameter inversions, such uncertainties are of limited value without knowing all the covariances. Uncertainties in parameters  $a$  and  $b$  might be large, but if they perfectly covary, our knowledge of the system is rather better than if they were entirely independent.

Here, I provide both a table of the 1 sigma uncertainties (Table 1) and the full correlation matrix of all of the variables (Figure 1). Note that within this dataset there are significant covariances. For example, the value of  $q_0$  of the stishovite phase is relatively poorly known (20% relative uncertainty), and a significant reason for this uncertainty is the pressure modification applied to the Zhang et al. (2021) data. The  $\Psi_{3a}$  and  $\Psi_{3b}$  parameters controlling the unit cell compression are also relatively poorly known but, as expected, trade off strongly against the diagonal elements of the compliance tensor.

Parameter	Value	Sigma	Relative uncertainty (%, 1 s.f.)
$V_0(Q = 0)$	1.400543e+01	5.448919e-03	0.04
$K_0(Q = 0)$	3.033375e+02	6.519069e-01	0.2
$K'_0(Q = 0)$	4.028431e+00	2.694942e-03	0.07
$\gamma_0(Q = 0)$	1.348008e+00	5.799027e-02	4
$q_0(Q = 0)$	1.600749e+00	3.648733e-01	20
$V_0(Q = 1)/V_0(Q = 0)$	9.938345e-01	3.917259e-04	0.04
$\Theta_0(Q = 1) - \Theta_0(Q = 0)$	1.762273e+01	1.450826e+00	8
$P_{tr}(T = T_{ref})$	4.996105e+01	4.658392e-01	0.9
$f_P$ (Zhang)	8.914754e-01	1.008448e-02	1
$f_P$ (Andrault)	9.897628e-01	9.292460e-03	0.9
$f_P$ (Wang)	9.878452e-01	1.934422e-02	2
$f_P$ (Nishihara)	9.957204e-01	9.930312e-02	10
$f_{P2}$ (Zhang)	2.929176e-13	1.688534e-13	60
$f_{P2}$ (Andrault)	-9.086680e-13	9.386737e-14	10
$f_{P2}$ (Wang)	-2.202689e-13	4.087520e-13	200
$f_{P2}$ (Nishihara)	1.559269e-12	5.419283e-12	300
$a_0(Q = 1)$	2.727799e-02	8.604317e-06	0.03
$b_0(Q = 1)$	2.856984e-02	8.175502e-06	0.03
$\Psi_{3a}$	2.103859e-01	5.713243e-03	3
$\Psi_{3b}$	-6.028139e-01	2.325219e-01	40
$\Psi_{3c}$	1.109034e+00	2.277065e-01	20
$\Psi_{3b2}$	8.868186e-05	5.407198e-05	60
$\Psi_{3c2}$	-1.096193e+01	1.600589e+00	10
$\Psi_{11a}$	3.248079e-01	3.338654e-02	10
$\Psi_{22a}$	8.376638e-01	4.109743e-02	5
$\Psi_{33a}$	4.930002e-01	4.586928e-03	0.9
$\Psi_{44a}$	1.119591e+00	1.698329e-02	2
$\Psi_{55a}$	1.209149e+00	1.761297e-02	1
$\Psi_{66a}$	9.492376e-01	4.459625e-03	0.5
$\Psi_{11b}$	-4.299730e-02	1.650548e-01	400
$\Psi_{33b}$	7.101613e-04	1.984595e-03	300
$\Psi_{44b}$	3.854751e-01	2.669142e+00	700
$\Psi_{66b}$	1.133123e-01	2.772369e+00	2000
$\Psi_{44c}$	9.745985e-01	9.863656e-01	100
$\Psi_{66c}$	9.973910e-01	3.224719e+00	300
$\Psi_{11b2}$	5.857416e-01	2.223387e-01	40
$\Psi_{33b2}$	2.130377e-01	2.127022e-02	10

**Table 1.** Parameters and their uncertainties for the full anisotropic model of stishovite and post-stishovite.

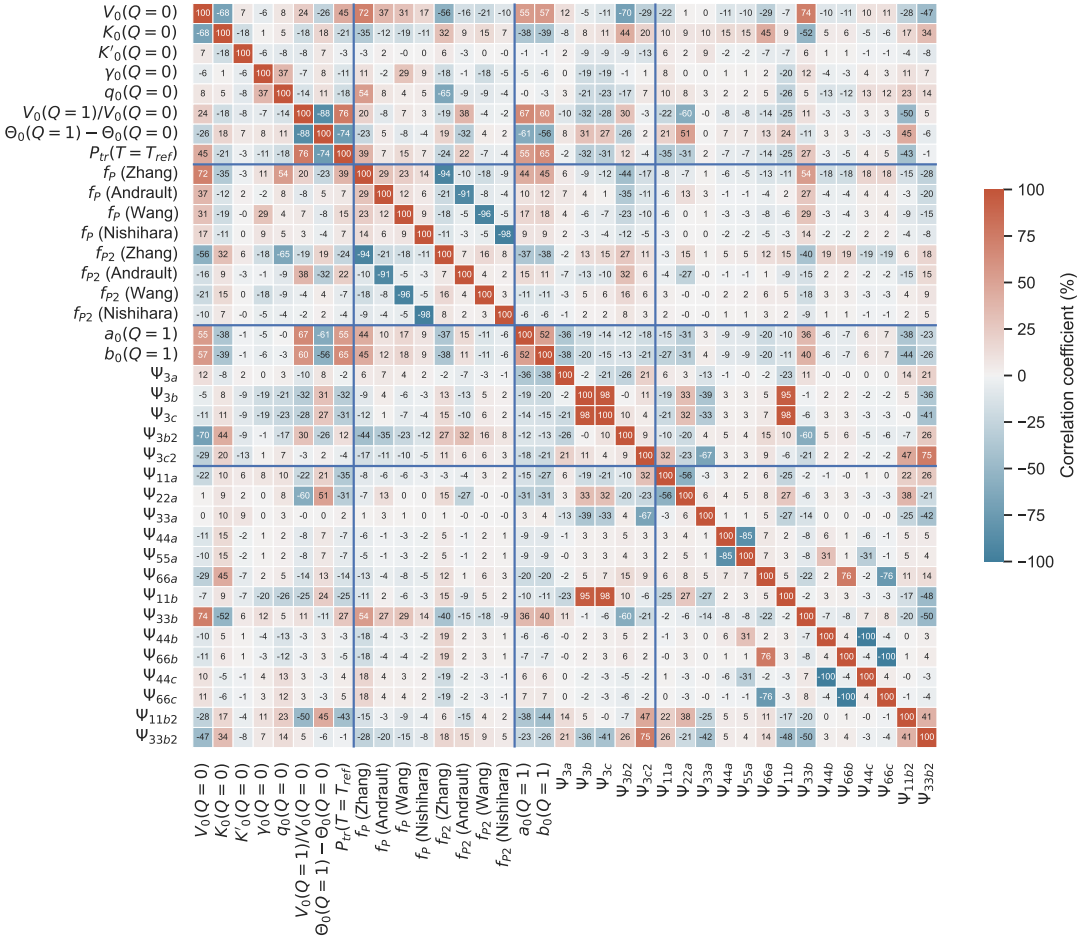


**Figure 1.** Correlation matrix of parameters used in the inversion for the full anisotropic model of stishovite and post-stishovite.

## 2 SEISMIC PROPERTIES

The figures on the following pages show the seismic properties of stishovite and post-stishovite at a series of pressures at a fixed temperature of 2200 K.

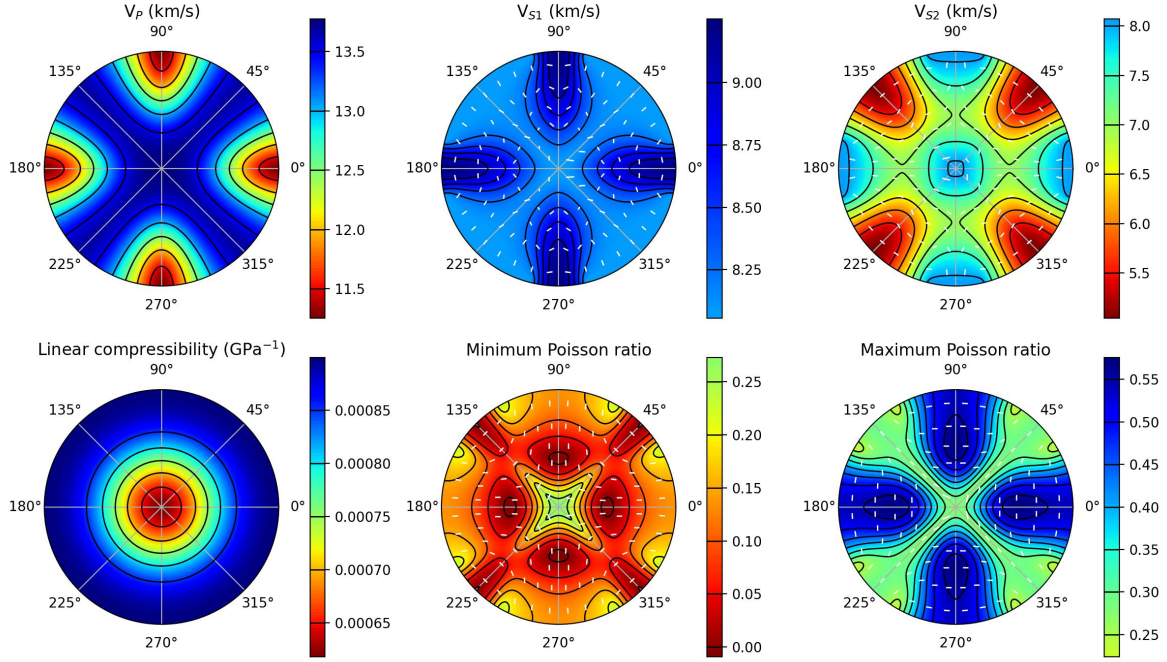


**Figure 2.** Modelled elastic properties at 37.27 GPa, 2200 K, which is 40 GPa lower pressure than the stishovite-post-stishovite transition. Upper hemisphere projection. S-wave velocities are plotted with white lines corresponding to the directions of particle motion. Minimum and maximum Poisson ratios are plotted at positions on the focal sphere that correspond to the axial propagation direction, with white lines corresponding to the lateral directions.

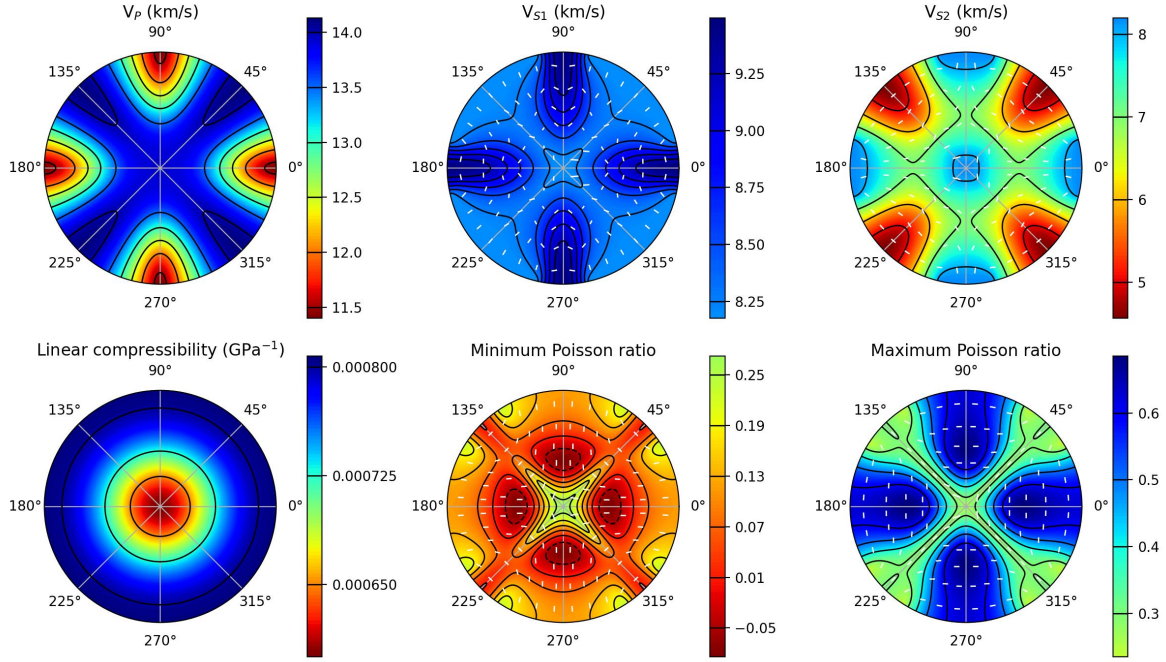


**Figure 3.** Modelled elastic properties at 47.27 GPa, 2200 K, which is 30 GPa lower pressure than the stishovite-post-stishovite transition. Symbols as in Figure 2.

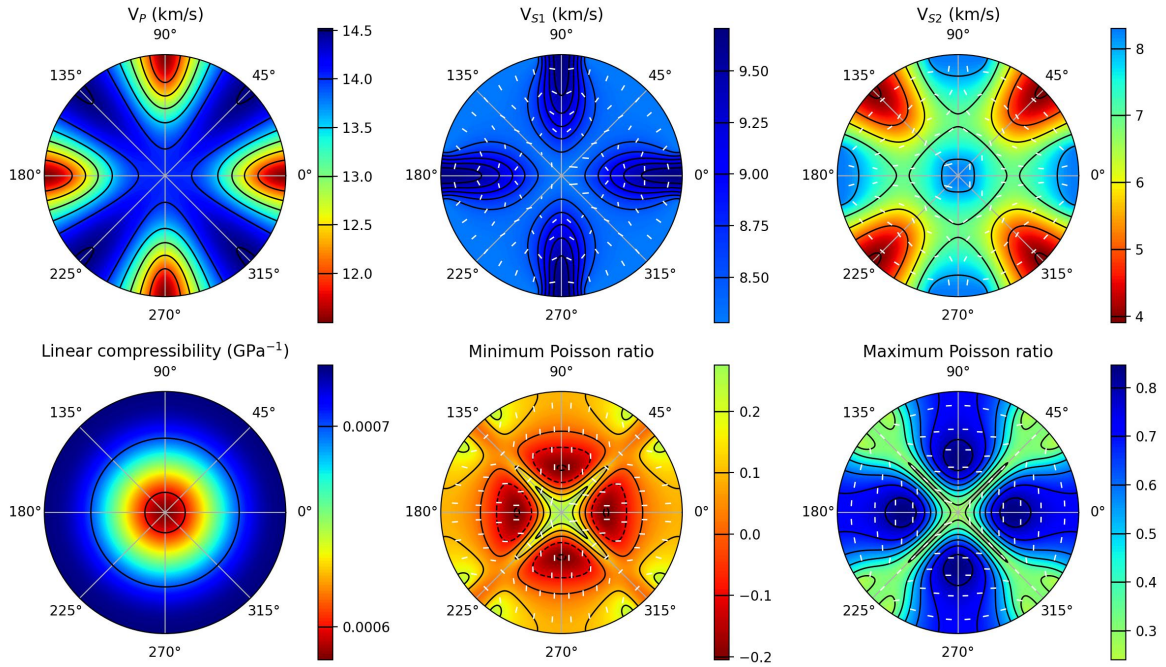


**Figure 4.** Modelled elastic properties at 57.27 GPa, 2200 K, which is 20 GPa lower pressure than the stishovite-post-stishovite transition. Symbols as in Figure 2.

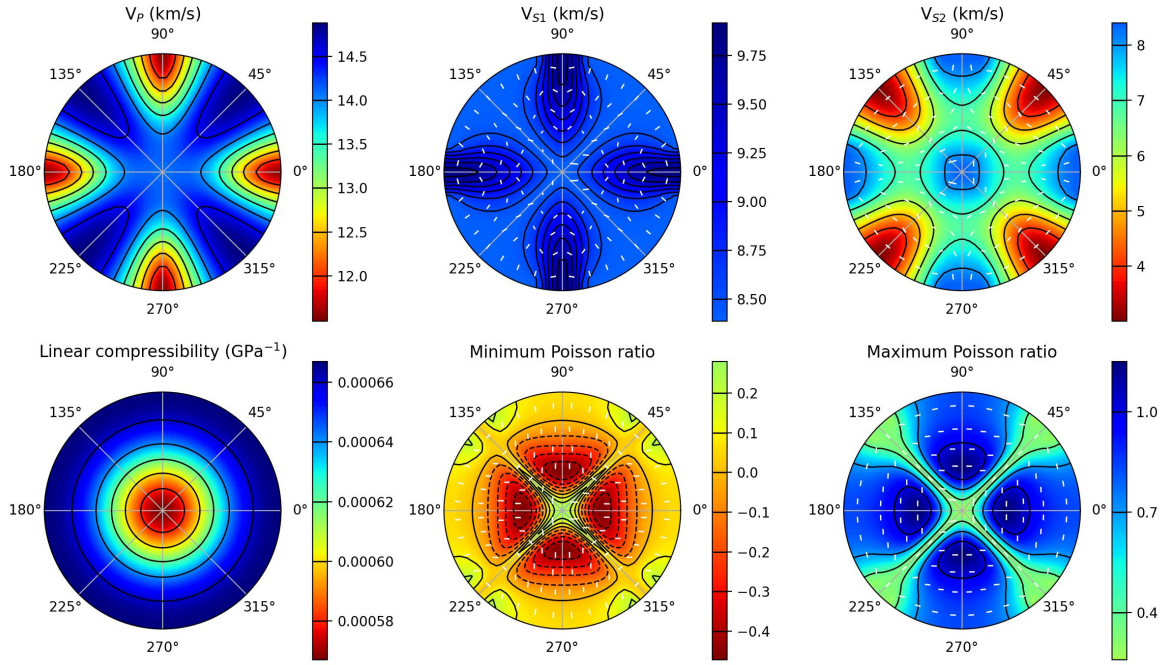


**Figure 5.** Modelled elastic properties at 67.27 GPa, 2200 K, which is 10 GPa lower pressure than the stishovite-post-stishovite transition. Symbols as in Figure 2.

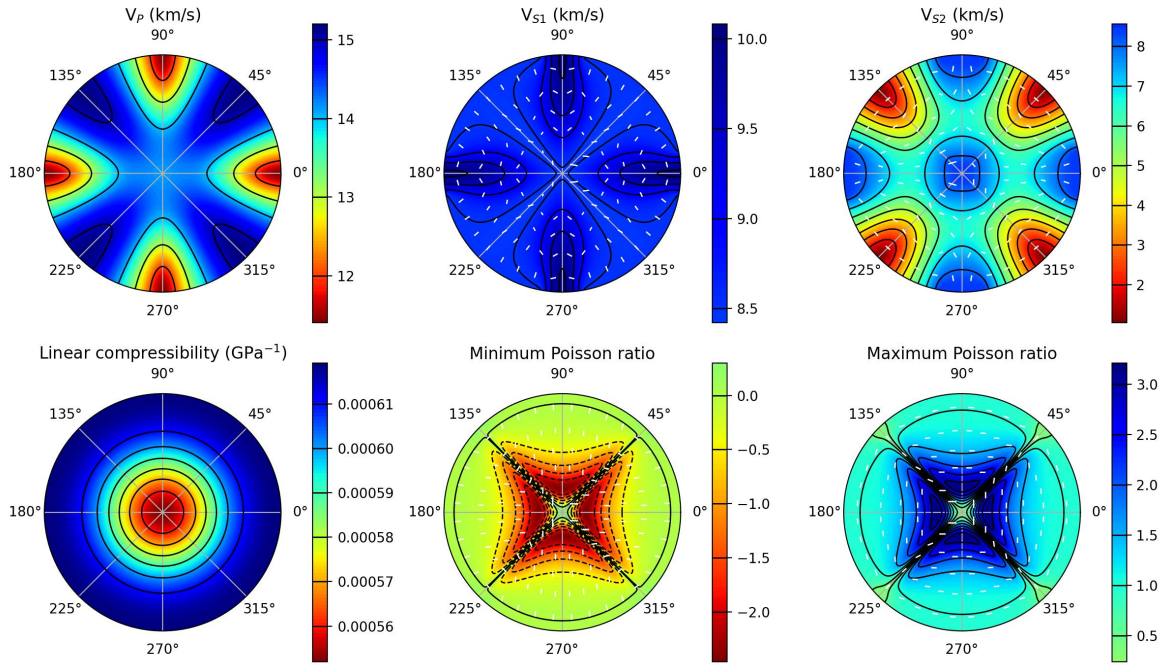


**Figure 6.** Modelled elastic properties at 76.27 GPa, 2200 K, which is 1 GPa lower pressure than the stishovite-post-stishovite transition. Symbols as in Figure 2.

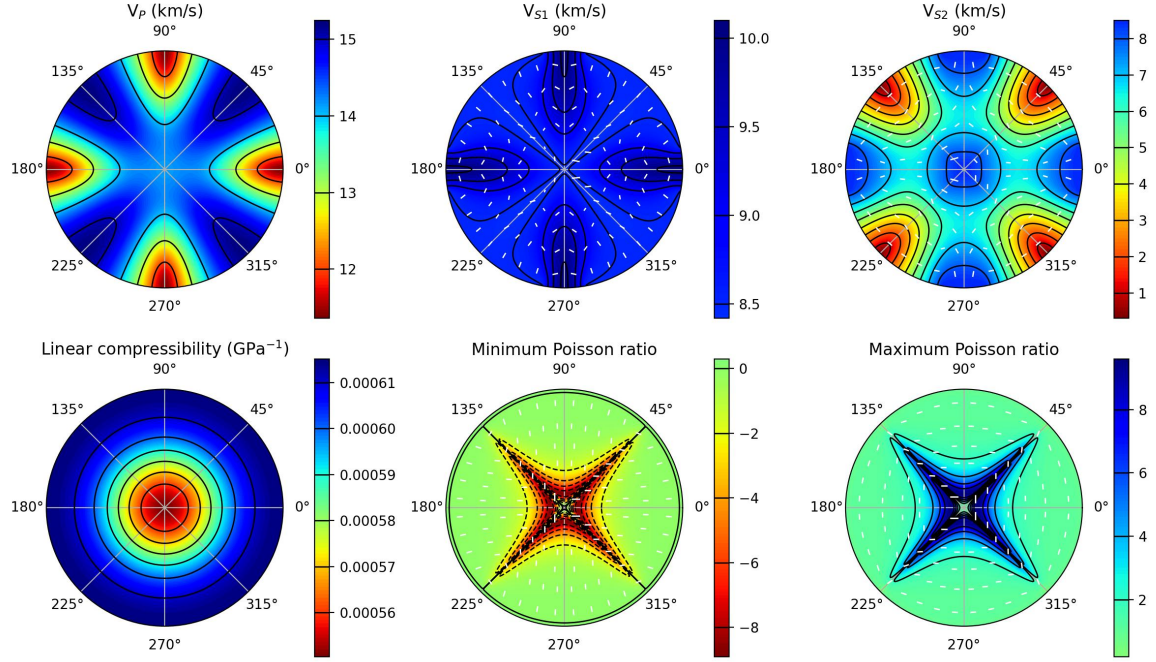


**Figure 7.** Modelled elastic properties at 77.17 GPa, 2200 K, which is 0.1 GPa lower pressure than the stishovite-post-stishovite transition. Symbols as in Figure 2.

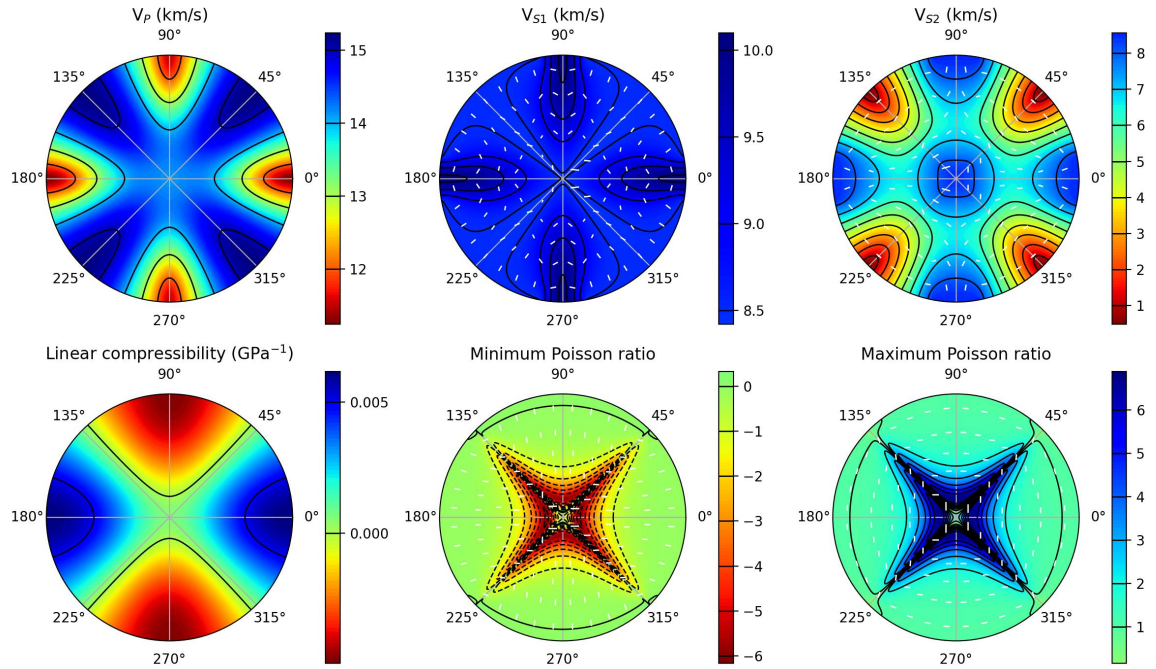


**Figure 8.** Modelled elastic properties at 77.37 GPa, 2200 K, which is 0.1 GPa higher pressure than the stishovite-post-stishovite transition. Symbols as in Figure 2.

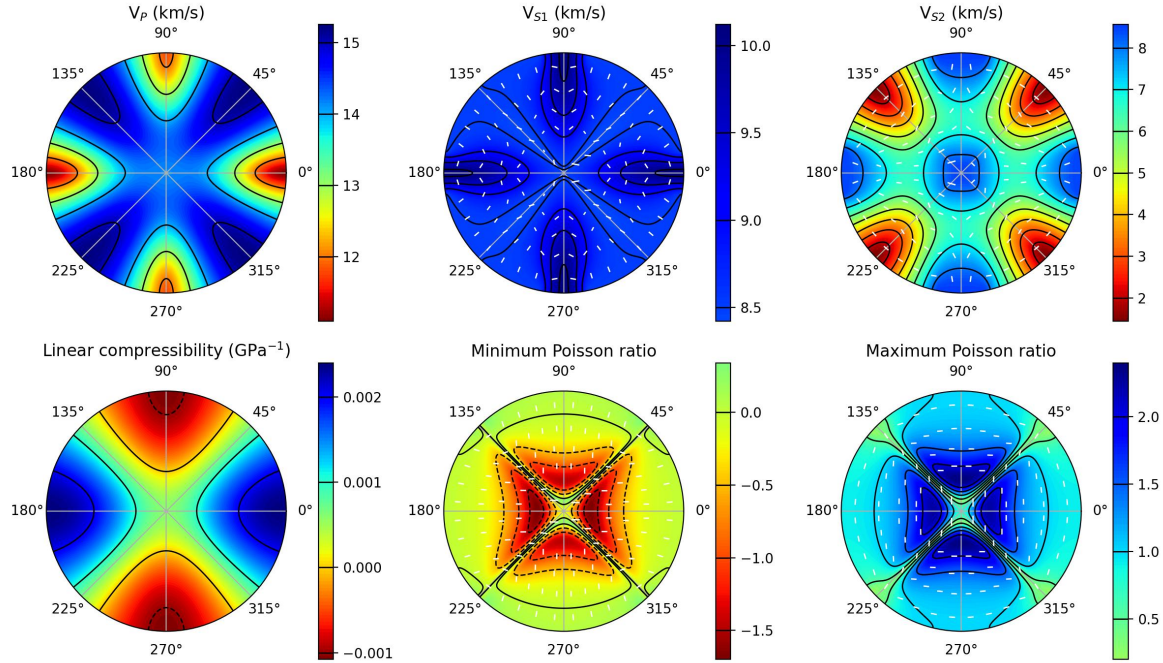


**Figure 9.** Modelled elastic properties at 78.27 GPa, 2200 K, which is 1 GPa higher pressure than the stishovite-post-stishovite transition. Symbols as in Figure 2.

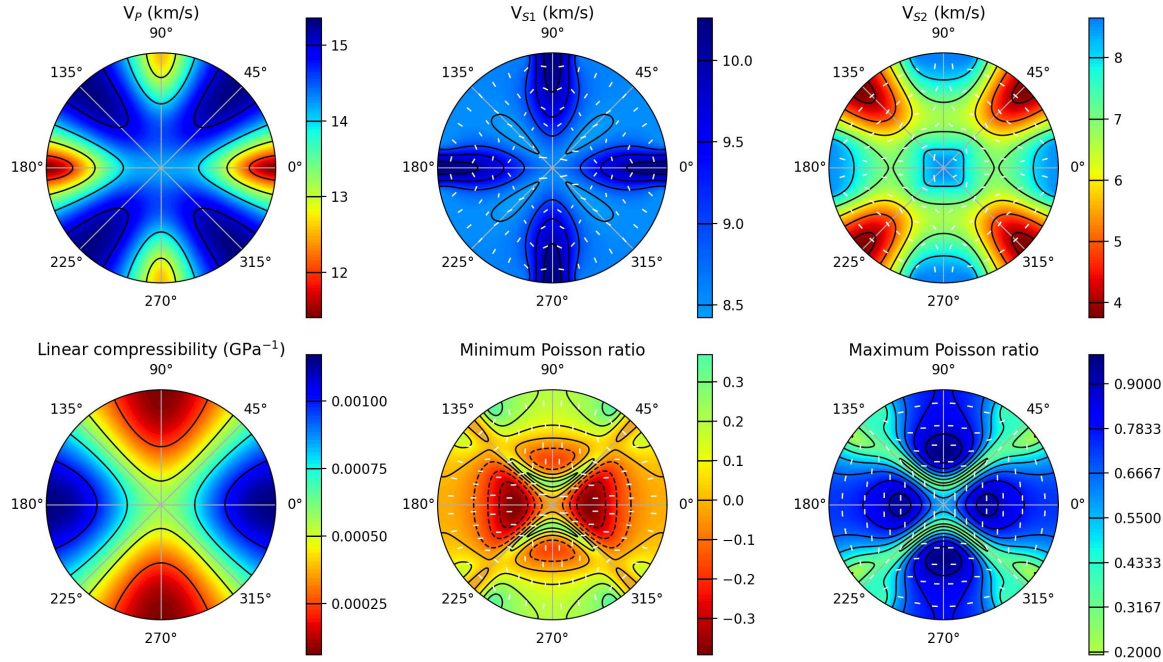


**Figure 10.** Modelled elastic properties at 87.27 GPa, 2200 K, which is 10 GPa higher pressure than the stishovite-post-stishovite transition. Symbols as in Figure 2.

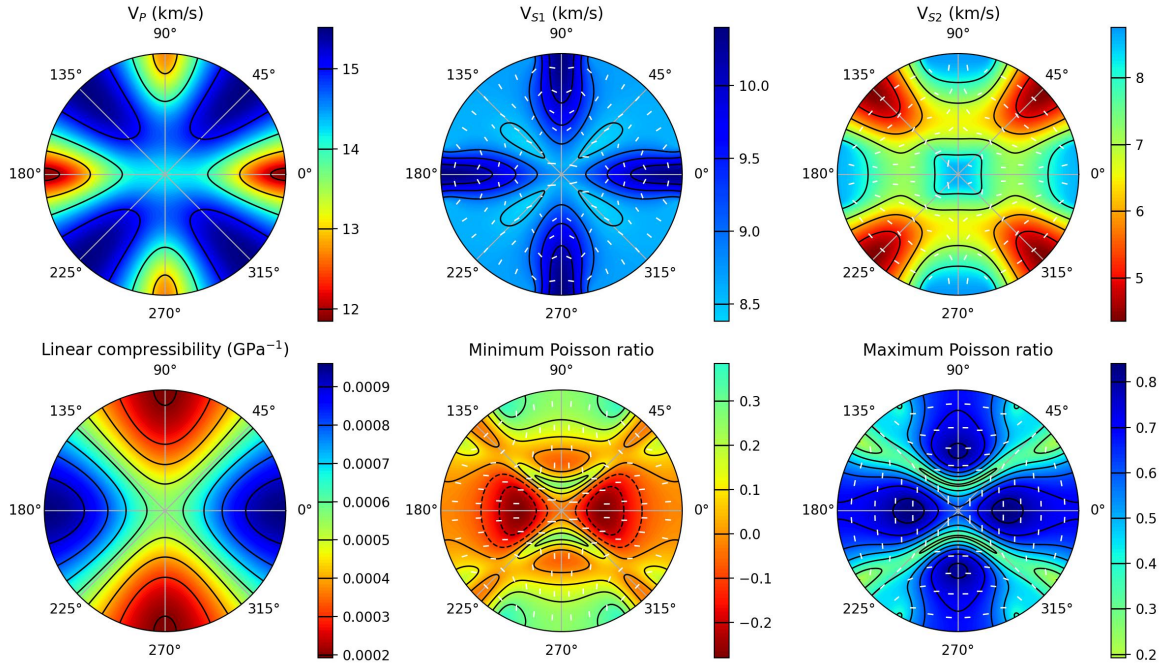


**Figure 11.** Modelled elastic properties at 97.27 GPa, 2200 K, which is 20 GPa higher pressure than the stishovite-post-stishovite transition. Symbols as in Figure 2.

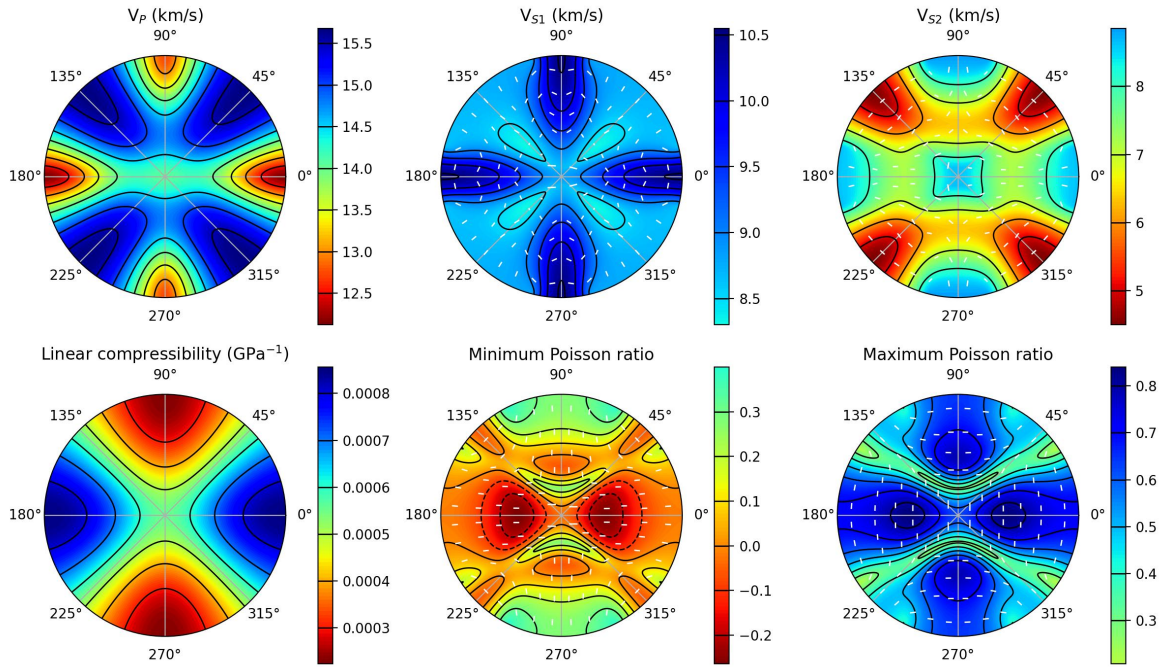


**Figure 12.** Modelled elastic properties at 107.27 GPa, 2200 K, which is 30 GPa higher pressure than the stishovite-post-stishovite transition. Symbols as in Figure 2.

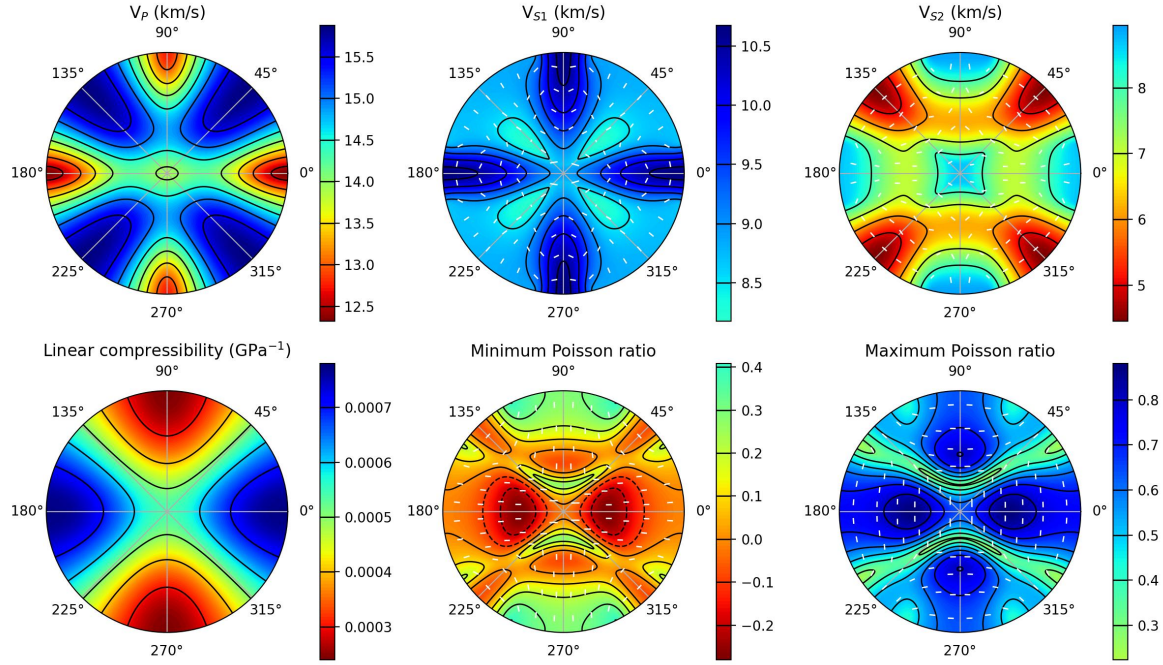


**Figure 13.** Modelled elastic properties at 117.27 GPa, 2200 K, which is 40 GPa higher pressure than the stishovite-post-stishovite transition. Symbols as in Figure 2.

### 3 A SLIGHTLY LONGER DESCRIPTION OF THE HISTORY OF SECOND ORDER PHASE TRANSITIONS

#### 3.1 Coupled models

Around the time Landau was developing his theory, other researchers were investigating piezoelectricity and ferroelectricity in crystals such as Rochelle salt, which undergo multiple phase transitions (Mueller, 1940; Devonshire, 1949). These phenomena can be modeled using energy density expressions involving strain infinitesimally small strains  $\varepsilon$  and polarization densities  $\mathcal{P}$  (e.g., Devonshire, 1949, their Equation 9.1):

$$\mathcal{F}(T, \varepsilon, \mathcal{P}) = \mathcal{F}_0(T) + \sum_{i,k} \mathbb{C}_{ik} \varepsilon_i \varepsilon_k + \frac{1}{2} \sum_j \chi_j(T) \mathcal{P}_j^2 + \frac{1}{2} \sum_{i,j} \xi_{ij} \mathcal{P}_i^2 \mathcal{P}_j^2 + \sum_{i,j,k} f_{ijk} \varepsilon_i \mathcal{P}_j \mathcal{P}_k \quad (1)$$

. Many parameters in these expressions are set to zero to reflect the symmetry of the crystal system. Partially differentiating the energy with respect to strain and polarization yields expressions for stress  $\sigma$  and electric field  $E$ . Setting these derivatives equal to the desired conditions results in a system of simultaneous equations. This system can have multiple solutions, and the stable solution corresponds to the one that minimizes  $\mathcal{F}$ .

Ginzburg (1945) presented a model for ferroelectric crystals that combined elements of both Landau-type and Devonshire-type models. He wrote the Gibbs energy as a function of electric field strength and polarization density:

$$\mathcal{G}(T, E, \mathcal{P}) = \mathcal{G}_0(T) + a(T) \mathcal{P}^2 + \frac{b(T)}{2} \mathcal{P}^4 - E \mathcal{P} \quad (2)$$

and minimized over the polarization  $\mathcal{P}$ . This expression is at first confusing; the Gibbs energy should not be a function of the polarization density, as it is a conjugate variable ( $\partial \mathcal{G} / \partial E = -\mathcal{P}$ ). The thermodynamic consistency of Equation 2 is made clearer by splitting it into two expressions:

$$\mathcal{G}(T, E, q) = \mathcal{G}_0(T) + a(T) q^2 + \frac{b(T)}{2} q^4 - E q \quad (3)$$

$$\left( \frac{\partial \mathcal{G}}{\partial E} \right)_T = -\mathcal{P} = -q \quad (4)$$

Expressions similar to Equation 2 were adopted by Levanyuk & Sannikov (1969, 1970, 1971) and termed “Landau-Ginzburg-Devonshire Theory”.

Further developments extended the theory to elastic effects (Dvořák, 1971; Höchli, 1972; Lüthi & Rehwald, 1981; Kityk et al., 2000). The expression for the energy density included terms involving the small strain tensor  $\varepsilon$ :

$$\mathcal{F}(T, \varepsilon, \mathbf{q}) = \mathcal{F}_0(T) + a_i q_i + b_{ij} q_i q_j + c_{ijk} q_i q_j q_k + \dots + \sum_{ij,m,n} \lambda_{ij,m,n} \varepsilon_i^m q_j^n + \frac{1}{2} \sum_{i,k} \mathbb{C}_{ik}^0 \varepsilon_i \varepsilon_k \quad (5)$$

where  $a, b, c, \lambda_{ij,m,n}, \mathbb{C}_{ik}^0, \dots$  are all potentially functions of temperature. The first three terms represent the classical Landau model, the penultimate term is a “strain-order coupling” term that is required to produce spontaneous strain, and the last term is an elastic term. In this expression,  $T$  and  $\varepsilon$  are natural variables of the system, and the equilibrium state under unstressed conditions ( $\sigma = 0$ ) can be found by setting  $\partial\mathcal{F}/\partial\varepsilon = \sigma = 0$  and minimizing over  $\mathbf{q}$ .

### 3.2 Elasticity at high pressure

The success of the coupled models in the previous section arises from the applicability of linear dielectric and linear elastic theory. Unfortunately, extending the theory to high pressure self-consistently requires dealing with nonlinear elasticity and finite strain (Tröster et al., 2002).

Some studies have attempted to use pressure as an independent variable, minimizing the Gibbs energy by varying the strain relative to the high-symmetry structure (Liakos & Saunders, 1982; Carpenter et al., 2000; Buchen, 2021):

$$\mathcal{G}(P, T, \varepsilon, \mathbf{q}) = \mathcal{G}_0(P, T) + aq^2 + bq^4 + \sum_{i,m,n} \lambda_{i,m,n} \varepsilon_i^m q^n + \frac{1}{2} \sum_{i,k} \mathbb{C}_{ik}^0 \varepsilon_i \varepsilon_k \quad (6)$$

Unfortunately, strain is not an internal variable, and so such minimizations are thermodynamically inconsistent. The problem can be illustrated through a specific model of the tetragonal stishovite to orthorhombic post-stishovite transition (Carpenter et al., 2000). This model predicts the equilibrium Gibbs energy (Figure 14a), volume (Figure 14b) and isothermal elastic stiffness tensor (their Figure 4) as a function of pressure at room temperature. The isothermal Reuss bulk modulus can be calculated in two ways from this model; (a) by inversion of the stiffness tensor:

$$K_{\text{TR}}^{-1} = \delta_{ij} \mathbb{C}_{ijkl}^{-1} \delta_{kl} \quad (7)$$

and (b) by differentiation of the Gibbs energy:

$$K_{\text{TR}} = - \left( \frac{\partial \mathcal{G}}{\partial P} \right) \left( \frac{\partial^2 \mathcal{G}}{\partial P \partial P} \right)^{-1} = -V \left( \frac{\partial P}{\partial V} \right) \quad (8)$$

In a thermodynamically consistent model, both methods should produce the same result, but in this model they do not (Figure 14c).

A variant of this model was proposed by Tröster et al. (2014, 2017). This model was formulated using the excess Helmholtz energy density, with small strain defined relative to the high-symmetry state:

$$\mathcal{F}_{\text{xs}}(\varepsilon, \mathbf{q}) = aq^2 + bq^4 + cq^6 + d_{ij} \varepsilon_{ij} q^2 + \sigma_{ij} \varepsilon_{ij} + \frac{1}{2} \mathbb{C}_{ijkl} \varepsilon_{ij} \varepsilon_{kl} \quad (9)$$

The equilibrium value of  $\mathcal{F}_{\text{xs}}$  is found by fixing the stress through  $\partial\mathcal{F}_{\text{xs}}/\partial\varepsilon$  and minimizing by varying  $q$ . Although thermodynamically self-consistent, this model still treats strain as small, and an equation

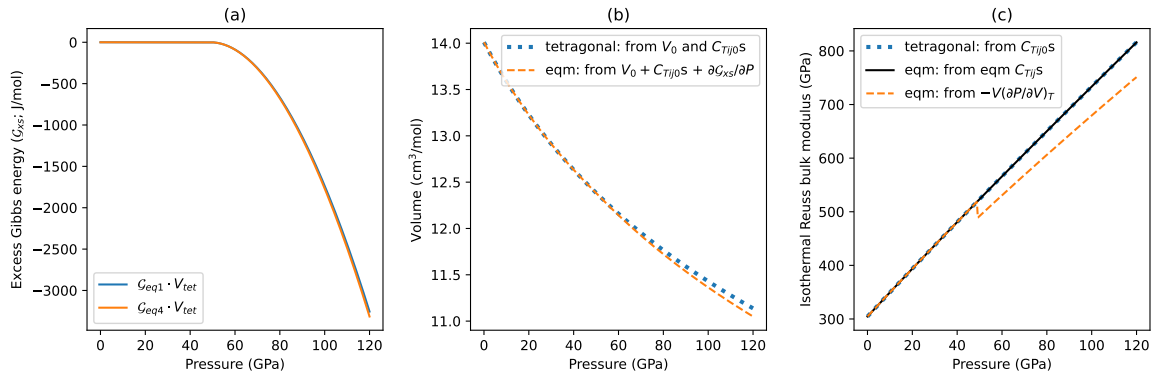


**Figure 14.** Predictions of properties through the tetragonal-orthorhombic stishovite to post-stishovite transition from the model of Carpenter et al. (2000) (a) The excess Gibbs energy. The two expressions given in Carpenter et al. (2000) differ very slightly in their values. (b) Volumes of the high-symmetry tetragonal phase (blue dotted line) and the equilibrium phase (orange dashed line) determined from the excess Gibbs energy. The standard state volume from Andrault et al. (2003) was used. (c) Reuss bulk modulus of the tetragonal phase (blue dotted line) and the equilibrium phase calculated from the reported moduli (black solid line), and the equilibrium volumes in (b) (orange dashed line).

of state is still required to determine the unit cell tensor and the elastic tensor in the high-symmetry state.

## References

- Andrault, D., Angel, R. J., Mosenfelder, J. L., & Le Bihan, T., 2003. Equation of state of stishovite to lower mantle pressures, *American Mineralogist*, **88**(2-3), 301–307.
- Buchen, J., 2021. *Seismic Wave Velocities in Earth's Mantle from Mineral Elasticity*, chap. 3, pp. 51–95, American Geophysical Union (AGU).
- Carpenter, M. A., Hemley, R. J., & Mao, H.-k., 2000. High-pressure elasticity of stishovite and the P42/mnm–Pnnm phase transition, *Journal of Geophysical Research: Solid Earth*, **105**(B5), 10807–10816.
- Devonshire, A., 1949. XCVI. Theory of barium titanate, *The London, Edinburgh, and Dublin Philosophical Magazine and Journal of Science*, **40**(309), 1040–1063.
- Dvořák, V., 1971. The origin of the structural phase transition in  $\text{Gd}_2(\text{MoO}_4)_3$ , *physica status solidi (b)*, **45**(1), 147–152.
- Ginzburg, V., 1945. On the dielectric properties of ferroelectric (seignettelectric) crystals and barium titanate, *Zh. eksp. teor. Fiz.*, **15**, 739.
- Höchli, U., 1972. Elastic constants and soft optical modes in gadolinium molybdate, *Physical Review B*, **6**(5), 1814.
- Kityk, A. V., Schranz, W., Sondergeld, P., Havlik, D., Salje, E. K. H., & Scott, J. F., 2000. Low-frequency superelasticity and nonlinear elastic behavior of  $\text{SrTiO}_3$ , *Physical Review B*, **61**(2), 946–956.
- Levanyuk, A. & Sannikov, D., 1969. Anomalies in dielectric properties in phase transitions, *Sov Phys JETP*, **28**, 134–139.
- Levanyuk, A. & Sannikov, D., 1970. Second order phase transitions close in temperature, *ZhETF Pisma Redaktsiiu*, **11**, 68.
- Levanyuk, A. & Sannikov, D., 1971. Phenomenological theory of dielectric anomalies in ferroelectric materials with several phase transitions at temperatures close together, *Sov. Phys. JETP*, **11**, 600–604.
- Liakos, J. & Saunders, G., 1982. Application of the Landau theory to elastic phase transitions, *Philosophical Magazine A*, **46**(2), 217–242.

- Lüthi, B. & Rehwald, W., 1981. Ultrasonic studies near structural phase transitions, in *Structural Phase Transitions I*, pp. 131–184, eds Müller, K. A. & Thomas, H., Springer Berlin Heidelberg, Berlin, Heidelberg.
- Mueller, H., 1940. Properties of Rochelle Salt, *Phys. Rev.*, **57**, 829–839.
- Tröster, A., Schranz, W., & Miletich, R., 2002. How to Couple Landau Theory to an Equation of State, *Phys. Rev. Lett.*, **88**, 055503.
- Tröster, A., Schranz, W., Karsai, F., & Blaha, P., 2014. Fully Consistent Finite-Strain Landau Theory for High-Pressure Phase Transitions, *Physical Review X*, **4**(3).
- Tröster, A., Ehsan, S., Belbase, K., Blaha, P., Kreisel, J., & Schranz, W., 2017. Finite-strain Landau theory applied to the high-pressure phase transition of lead titanate, *Phys. Rev. B*, **95**, 064111.
- Zhang, Y., Chariton, S., He, J., Fu, S., Prakapenka, V. B., & Lin, J.-F., 2021. Ferroelastic post-stishovite transition mechanism revealed by single-crystal x-ray diffraction refinements at high pressure, *Earth and Space Science Open Archive*, p. 26.

This paper has been produced using the Blackwell Scientific Publications GJI L<sup>A</sup>T<sub>E</sub>X2e class file.